Impact of Virtual Power Plants on Power System Short-Term Transient Response

Weilin Zhong, Mohammed Ahsan Adib Murad, Muyang Liu, Federico Milano
AMPSAS, School of Electrical & Electronic Engineering, University College Dublin, Ireland
{weilin.zhong, mohammed.murad, muyang.liu}@ucdconnect.ie, federico.milano@ucd.ie

***Abstract*—This paper studies the impact of coordinated and non-coordinated frequency control of Virtual Power Plants (VPPs) on power system transients. A realistic modelling of the communication system within the VPP is also taken into account. The case study considers a modified version of the WSCC 9-bus test system with inclusions of a VPP with distributed generations and, discusses the performance of the coordinated frequency controller in the VPP. All simulations are performed considering both deterministic and stochastic variations of the wind and voltage-dependent loads.**

***Index Terms*—Virtual power plant (VPP), communication delays, distributed energy resources (DERs), power system dynamic, energy storage system (ESS), frequency control.**

I. Introduction

A. Motivation

Virtual Power Plants (VPPs) and, in particular, the efficient utilization of the Distributed Energy Resources (DERs) in VPPs have become a timely research topic. Most studies on VPPs, however, focus exclusively on the operation and economic aspects [1]–[3]. The transient behavior of VPPs as well as their impact on the overall power system dynamic response, on the other hand, are not thoroughly studied. Moreover, since the coordination of DERs requires the exchange of measurements and control signals among controllers in a centralized VPP [4], delays are inevitably introduced. This paper focuses on the primary frequency control of VPPs and compares different DER coordination strategies and communication systems delays.

B. Literature Review

1) Virtual Power Plant: VPP is still in an early development stage, and the definition of VPP has not yet been unified [5]. In the FENIX project, the concept of VPP is defined as a *flexible aggregation of DERs*, e.g., wind turbines, solar photovoltaic generation, and energy storage systems. The VPP control consists of collecting the characterizing parameters from the DERs and regulating them, taking into account network characteristics, e.g., topology and losses [6]. In [7], VPPs are defined as *heterogeneous entities of multi-technology and multi-site*; while in [8], a VPP is *an aggregation of many diverse DERs, which can be connected to different points of the medium voltage distribution network dispersedly*. Also, a VPP can be considered as an autonomous, isolated microgrid [9]. In this paper, a VPP is considered as the aggregation of geographically dispersed DERs installed in a distribution grid, including Distributed Generators (DGs) and Energy Storage Systems (ESSs).

2) Virtual Power Plant control strategy: VPPs can be controlled with a distributed or centralized strategy [4]. Reference [10] proposes a distributed control strategy for the multiple DGs in a VPP, in which the DGs can adaptively adjust the output power of VPP and reach an optimal point through local communication networks. In [11], a definition for the service-centric VPP is given, and the solution of the congestion relief service via optimal adjusting the active and reactive power in the VPP to enhance the integration of wind and solar power is also developed. Reference [12] proposes a novel technique for voltage regulation along a distribution line by a VPP, which focuses on the restoration of bus voltages within the standard limitations. Two operation models are presented in [13], including VPP dispatch model based on time-of-use pricing mechanism, and the game-theoretic dispatch model for multiVPP based on the optimal results of VPP dispatch. Reference [14] proposes a decentralized cooperative frequency control for autonomous VPPs with communication constraints. Compared with the centralized approach that consists in collecting the information from ESSs and DGs in a single control centre, in a cooperative (distributed) control, each DER shares its information only with neighboring DERs [15].

3) Virtual Power Plant Communication: Similar to the VPP control strategy, the communication strategy in VPP can also be divided into centralized and decentralized. Centralized communication strategy has a high requirement for the communication network of transferring all individual DERs information, while the decentralized communication shows some advantages when the DERs in VPP have communication limitations. Reference [16] proposes the communication, information, and functional requirements of VPP for grid services using the IEC 61850 standard. A distributed dispatch method based on the primal-dual sub-gradient algorithm is proposed in [17]. This method maximizes the profit of VPP by coordination individual decision-making of DERs in the VPP via limited communication, which has a similar performance to the

This work was supported by Science Foundation Ireland, by funding W. Zhong and F. Milano under project ESIPP, Grant No. SFI/15/SPP/E3125, and M. A. Adib Murad, M. Liu and F. Milano under project AMPSAS, Grant No. SFI/15/IA/3074; and by the European Commission by funding F. Milano under project EdgeFLEX, Grant No. 883710.

centralized dispatch. In [14], a decentralized communication strategy is proposed. In this strategy, a "global" quantity, i.e. the measurement of the total generated active power, is shared between every two neighbor DERs, which avoids the communication constraints.

C. Contributions

The contributions of this paper are twofold, as follows.

- A centralized, coordinated frequency control strategy for DERs is included in a VPP, and the impact of such strategies on the overall transient behavior is studied considering both deterministic and stochastic simulations.
- It presents an in-depth analysis of the impact of delays on overall dynamic response.

D. Organization

The remainder of the paper is organized as follows. Section II outlines the frequency control schemes of ESSs, wind turbines, Solar Photo-Voltaic Generation (SPVG), and describes the basic structure of the Phase-Locked Loop (PLL), which is utilized to estimate network frequency variations. Section III-A presents the design of the coordinated frequency control scheme for ESSs, whereas Section III-B describes the communication delay model used in the paper. Section IV describes the stochastic load and wind speed models considered in this study. Section V discusses in detail the case study based on a modified version of the well-known WSCC 9-bus, 3-machine test system. The VPP is modelled based on a real-world Irish distribution system. Finally, Section VI draws conclusions and outlines future work.

II. Frequency Controllers of the DERs

This section outlines the frequency control schemes of ESSs, wind turbines, SPVGs and the PLLs.

A. Energy Storage Systems

ESSs are widely utilized for fast active power support in a power system, and several simplified models of ESS has been proposed in recent years [18]. In this paper, we use the active power control scheme proposed in [19], which is shown in Fig. 1. The input signal of this control scheme is

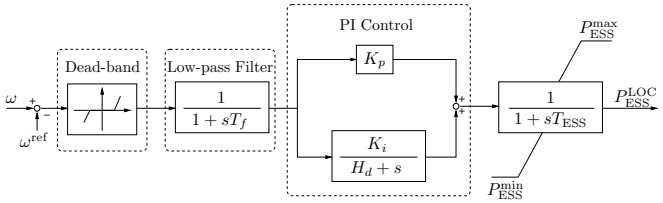

Fig. 1: The frequency control scheme of an ESS.

the deviation of the measured frequency (ω), with a reference frequency (ω^{ref}). A dead-band and low-pass filter (LPF) blocks are included to reduce the sensitivity of the input signal, and to filter out noises. The PI controller is composed of a proportional gain K_p, an integral gain K_i, and an integral deviation coefficient H_d emulated by the droop gain. Finally the output is achieved through an anti-windup first-order lag filter.

B. Wind Turbines

The most common approach of frequency control of wind turbines is to couple the output of the Maximum Power Point Tracking (MPPT) with the deviation of the measured frequency (droop control) or/and the Rate of Change of Frequency (RoCoF) control [20]. Fig. 2 depicts the primary controller of wind turbines considered in this paper.

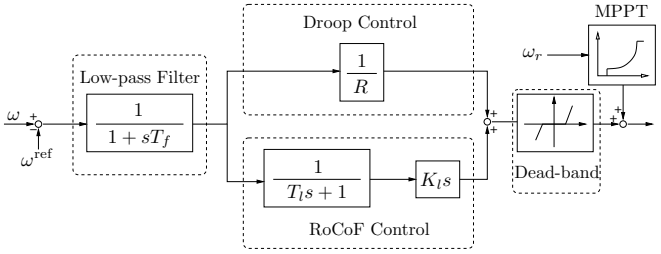

Fig. 2: The droop and RoCoF controllers connected to the MPPT of wind turbine.

In this scheme, the RoCoF control is faster and mainly acts instantly after any disturbance, while the droop control is slower and reduces the frequency deviations [21]. The resulting frequency control signal is then added to the output of the MPPT.

C. Solar Photo-Voltaic Generation

The connection of SPVG with the grid is similar to wind turbines [22]. The SPVG frequency control scheme utilized in this paper is shown in Fig. 3.

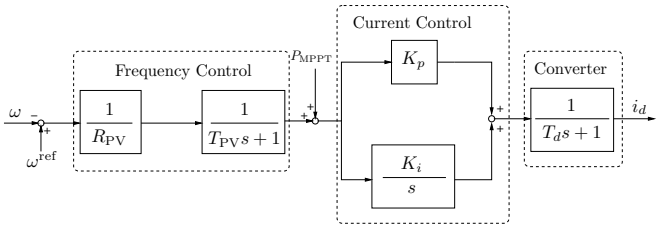

Fig. 3: Frequency control scheme of the SPVG.

In this scheme, the droop control is a series combination of droop gain and a low pass filter. The output signal of the frequency controller is then added to the active power reference of the MPPT, and fed to a PI controller. Finally the SPVG converter generates the d-axis current i_d.

D. Phase-Looked Loop

PLLs are widely-used for the synchronization with the ac grid of the power electronic devices included in the DERs. As a byproduct of the synchronization, a PLL can also provide the estimation of the bus frequency at which it is connected. There are several PLL implementations. We consider the Synchronous Reference Frame PLL (SRF-PLL) which is one of the most commonly utilized [21], [23]. The scheme of the SRF-PLL is shown in Fig. 4.

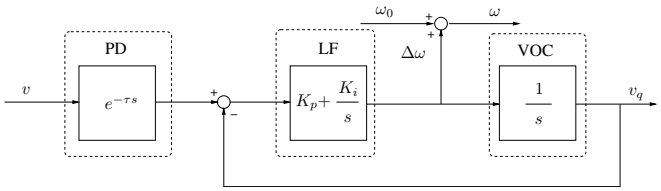

Fig. 4: The scheme of the SRF-PLL.

The SRF-PLL consists of three main components: a Phase Detector (PD), a Loop Filter (LF), and a Voltage Oscillator Controller (VOC). The PD measures the bus voltage (v) at the point of connection through a constant delay. The LF is a PI controller, which produces the estimation of the bus frequency deviation $\Delta\omega$. Then the frequency estimation ω is obtained by adding the system fundamental frequency ω_0 and the $\Delta\omega$.

III. Coordinated Control Scheme

This section describes the proposed centralized frequency control for DERs.

A. Coordinated Frequency Control Scheme for ESS

We consider the primary frequency control of the VPP exclusively. The main objective of the coordination is to guarantee a fast frequency response of the VPP by means of the active power control by the ESSs. A centralized control strategy is adopted to ensure a consistent response from all the resources in the VPP. The strategy is illustrated in Fig. 5.

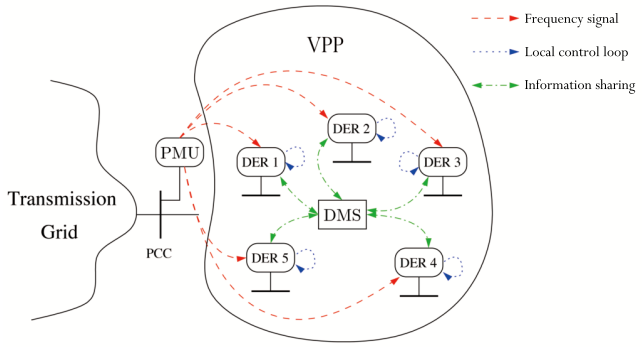

Fig. 5: Illustration of the coordinated control scheme.

The frequency is measured through a phasor measurement unit (PMU) at the point of the VPP coupled with the transmission grid (TG). All DERs use the same frequency signal as an input signal in their local control loop, which has been discussed in Section II. Then the information of each DER, i.e. the active power output, is sent and collected by a data management system (DMS) located within the VPP. Note that during the data transmitted from PMU to DERs, or/and from DERs to DMS, the communication delay related to the measurement and dispatch of the data should be considered.

The power generated by the VPP is obtained by summing up the production of each DER devices included in the VPP. The coordinated control of DERs and ESSs is achieved through the primary frequency control support provided by the ESS, based on the information shared from the DERs included in the VPP. With this aim, a feedback signal is added to the local control loop of ESS to consider the active power outputs from wind turbines and SPVGs. Fig. 6 illustrates the control scheme of the ESS with a coordinated signal from the DERs of the VPP.

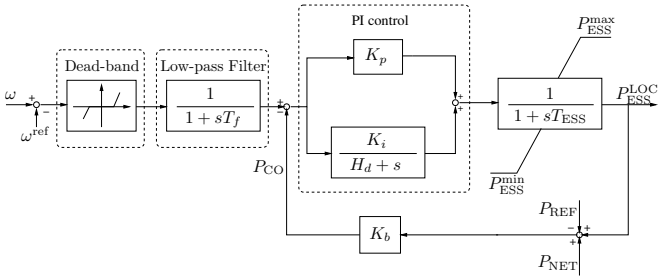

Fig. 6: Scheme of the ESS with coordinated signal control.

The process of the control scheme can be expressed as:

$$\begin{cases} P_{\text{CO}} & = K_b * (P_{\text{ESS}}^{\text{LOC}} + P_{\text{NET}} - P_{\text{REF}}), \\ P_{\text{NET}} & = \sum_{i=1}^{l} P_{\text{ESS}}^{i} + \sum_{j=1}^{m} P_{\text{WIND}}^{j} + \sum_{k=1}^{n} P_{\text{SOLAR}}^{k} \\ & \quad -P_{\text{LOSS}}^{\text{TOT}} - P_{\text{LOAD}}^{\text{TOT}} - P_{\text{INJ}}^{\text{TOT}}, \\ & \quad i = 1, 2, ..., l; j = 1, 2, ..., m; k = 1, 2, ..., n \end{cases} \tag{1}$$

where P_{CO} is the feedback signal through a proportional gain K_b, $P_{\text{ESS}}^{\text{LOC}}$ is the active power output from the local ESS, P_{NET} is the net active power of the VPP, which is sending from the control center, $\sum_{i=1}^{l} P_{\text{ESS}}^{i}$ is the total active power output from all the ESSs except the local ESS, P_{REF} is the initial reference set-point equal to the P_{NET}, $\sum_{j=1}^{m} P_{\text{WIND}}^{j}$ and $\sum_{k=1}^{n} P_{\text{SOLAR}}^{k}$ are the sum output of the active power from the DERs in VPP. Finally $P_{\text{LOSS}}^{\text{TOT}}$, $P_{\text{LOAD}}^{\text{TOT}}$ and $P_{\text{INJ}}^{\text{TOT}}$ are the total active power losses and load in VPP, and the injection from/to the transmission grid, respectively.

B. Communication Delay Model

Centralized control is expected to introduce delays and communication issues, e.g. packet dropout, which can limit the ability of the VPP to stabilize the grid. The time delay in the power systems can consider as the following set of Delay Differential-Algebraic Equations (DDAEs) [24]:

$$\begin{aligned} \dot{\boldsymbol{x}} &= \boldsymbol{f}(\boldsymbol{x}, \boldsymbol{y}, \boldsymbol{x}_d, \boldsymbol{y}_d, \boldsymbol{u}) \\ \boldsymbol{0} &= \boldsymbol{g}(\boldsymbol{x}, \boldsymbol{y}, \boldsymbol{x}_d, \boldsymbol{y}_d, \boldsymbol{u}) \ , \end{aligned} \tag{2}$$

where $\boldsymbol{f}$ and $\boldsymbol{g}$ are the differential and algebraic equations respectively; $\boldsymbol{x}$, $\boldsymbol{y}$, $\boldsymbol{x}_d$, $\boldsymbol{y}_d$ and $\boldsymbol{u}$ are the state, algebraic, delayed state, delayed algebraic and input variables respectively.

The delayed control signal, in this case, is the remote active power signal from the VPP, say P_{NET}:

$$P_{\text{NET},d} = P_{\text{NET}} * (t - \tau(t)), \tag{3}$$

where the delay $\tau(t)$ can be considered as a Wide-Area Communication (WAC) delay [25], and formulated as:

$$\tau(t) = \tau_f + \tau_p(t) + \theta(t), \tag{4}$$

where τ is the total delay, τ_f is the fixed delay associated with transducers used and data processing, τ_p is the transmission delay, and θ is the associated random jitter.

In an ideal WAC network, the transmission delay τ_p for each data packet has an identical constant period:

$$T = t_{k+1} - t_k \ , \tag{5}$$

where t_k is the time that k-th data packet arrives. The transmission delay at a specific time t can be derived as:

$$\tau_p(t) = t - t_k \ . \tag{6}$$

In a real-world WAC network, the $k+1$-th packet can be lost. If the packet drop-out occurs, the Zero-Order Holder (ZOH) will hold the latest state as the feedback signal to the controllers until the next packet has been received, which means that the delay of the last lost packet is automatically added to the next packet [26], [27].

In this study, the WAC delay is generated by a co-simulation software proposed in [28], the transmission delay is:

$$\tau_p = \tau_{po} + L/R, \tag{7}$$

where τ_{po} is the propagation delay decided by the transmission medium, L is the size of each packet, and R is the data rate in the transmission channel. The θ in (4) considers the network-induced issues, e.g. noise, network topology, routing protocol, and background traffic.

IV. Stochastic Models

This section outlines the stochastic models of loads and wind speeds considered in this study. The stochastic variations are modeled by means of the following Itô-type differential equation:

$$dx(t) = a(x(t), t)dt + b(x(t), t)dw(t), \tag{8}$$

where $x(t)$ and $w(t)$ are the variable affected by noise and a standard Wiener process respectively; $a(x(t), t)$ and $b(x(t), t)$ are the drift and the diffusion terms respectively. Both Gaussian and non-Gaussian processes are appropriately considered by (8), therefore is applicable to model load power variations and wind speed fluctuations [29].

A. Stochastic Voltage Dependent Load Model

The stochastic voltage dependent load model is:

$$\begin{aligned} p_L(t) &= (-p_{L0} + \eta_p(t))(v(t)/v_0)^\gamma \\ q_L(t) &= (-q_{L0} + \eta_q(t))(v(t)/v_0)^\gamma \\ \dot{\eta}_p(t) &= \alpha_p(\mu_p - \eta_p(t)) + b_p\xi_p \\ \dot{\eta}_q(t) &= \alpha_q(\mu_q - \eta_q(t)) + b_q\xi_q, \end{aligned} \tag{9}$$

where p_{L0} and q_{L0} are the active and reactive powers at the the nominal voltage v_0; $v(t)$ is the voltage magnitude of the bus where the load is connected; and γ is the power exponent; the α terms are the speed at which the stochastic variables η are "attracted" towards the mean values μ, and the b terms represents the volatility of the processes.

B. Stochastic Wind Model

To emulate the wind speed, $a(\cdot)$ and $b(\cdot)$ in (8) must be defined so that the probability distribution of $x(t)$ is a Weibull process [30]. The resulting drift and diffusion terms are:

$$\begin{aligned} a(x(t)) &= -\alpha \cdot (x(t) - \mu_{\mathrm{W}}) \\ b(x(t)) &= \sqrt{b_1(x(t)) \cdot b_2(x(t))} \ , \end{aligned} \tag{10}$$

where α is the autocorrelation coefficient; μ_{W} is the mean of the Weibull distribution; and

$$b_1(x(t)) = \frac{2 \cdot \alpha}{p_{\mathrm{W}}(x(t))}$$

$$b_2(x(t)) = \lambda \cdot \Gamma\left(1 + \frac{1}{k}, \left(\frac{x(t)}{\lambda}\right)^k\right) - \mu_{\mathrm{W}} \cdot e^{-(x(t)/\lambda)^k} \ ,$$

where $p_W(\cdot)$ is the Probability Density Function (PDF) of the Weibull distribution; $\Gamma(\cdot, \cdot)$ is the incomplete Gamma function; k and λ are the shape and scale parameters of the Weibull distribution, respectively.

V. Case Study

The case study considers a modified version of the well-known WSCC 9-bus, 3-machine system (see [31]). In this system, the load at bus 6 in the original network has been replaced with a VPP. The VPP includes an 8-bus, 38 kV distribution system [32].

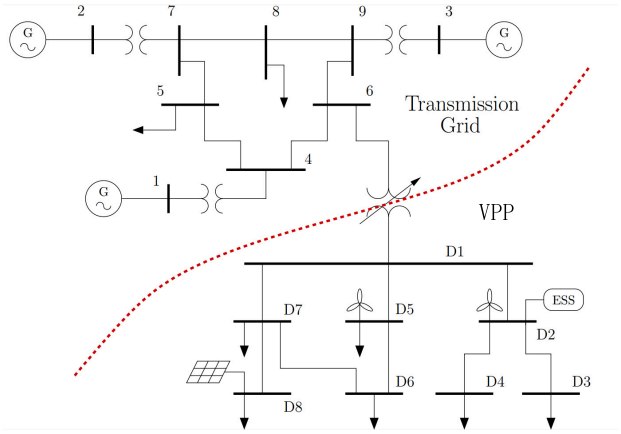

Fig. 7: Modified WSCC 9-bus, 3-machine system with a VPP.

A. Virtual Power Plant

The structure of the VPP is depicted in Fig. 7, and the composition is described as follows.

- The VPP is connected with the transmission system through an automatic Under-Load Tap Changer (ULTC) type step down transformer.
- One solar PV plant, two wind power plants, one ESS are connected at buses D8, D5, D2, and D2, respectively. Each DER utilizes the bus frequency signal by an SRF-PLL installed at Bus D1, for frequency control. The initial active power generation of the wind power plants and the solar PV plant are 15 MW each, whereas the power rate of the ESS is 6.75 MW.

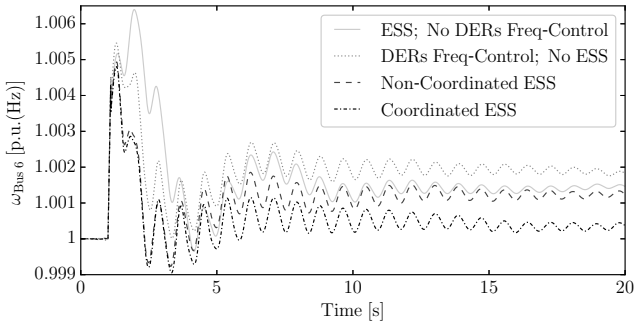

Fig. 8: Frequency response at bus 6 following the contingency.

- The total active and reactive power consumption of loads in the VPP is 0.578 MW and 0.117 MVar, respectively.

B. Simulation Scenarios

Two scenarios have been studied in this section. First, Subsection V-C studies the impact of VPP on power system transient response considering four types of VPPs: (i) without DERs frequency control but with the ESS controlling the frequency; (ii) without ESS but with DERs controlling the frequency; (iii) with non-coordinated DERs and ESS and (iv) with coordinated ESS and DERs, considering both deterministic and stochastic simulations. Subsection V-D focuses on the impact of communication delay of the remote control signal transmitted in different levels of communication networks.

For all scenarios, the contingency is a three-phase fault at bus 7 at $t = 1$ s, cleared after 100 ms by opening the line connecting buses 5 and 7. All simulations are solved using Python-based software tool DOME [33].

C. Impact of Coordinated Control of VPP

The performance of the system for the different control schemes is studied by comparing the frequency at bus 6. Fig. 8 shows the frequency response following the disturbance for the four scenarios. If the ESS is installed in the VPP, the steady-state frequency error is lower compared to the case without the ESS, however not zero due to limited capabilities of the ESS and the fact that the Automatic Generation Control (AGC) is not considered in the simulation. On the other hand, the frequency shows the maximum deviation for the case where DERs do not participate to the frequency control. The best dynamic response is achieved through a coordinated control of DERs and ESS.

The active power output of DERs and the active power absorption of the ESS are shown in Fig. 9 with non-coordinated and coordinated ESS control. Due to the coordination of the DERs outputs, the ESS reaches its maximum power output limit after the contingency.

The impact of the limit of the energy capacity of the ESS is studied next by performing a simulation with a longer time scale and assuming that the ESS is at a 70% state of charge before the contingency. Fig. 10 shows the frequency at bus 6 for the scenarios without ESS and with ESS with coordinated

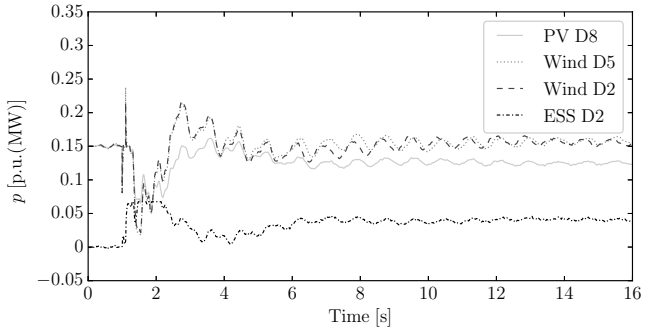

(a)

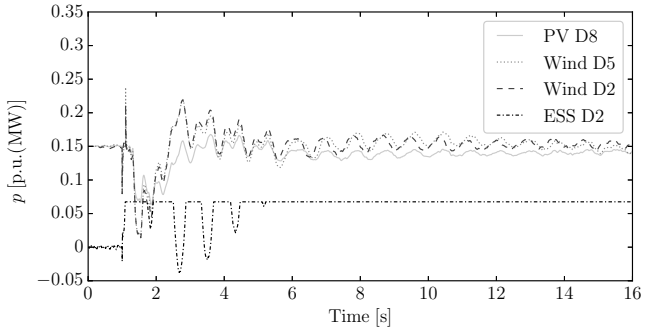

(b)

Fig. 9: Active power output of the DERs in VPP: (a) with non-coordinated ESS (b) with coordinated ESS.

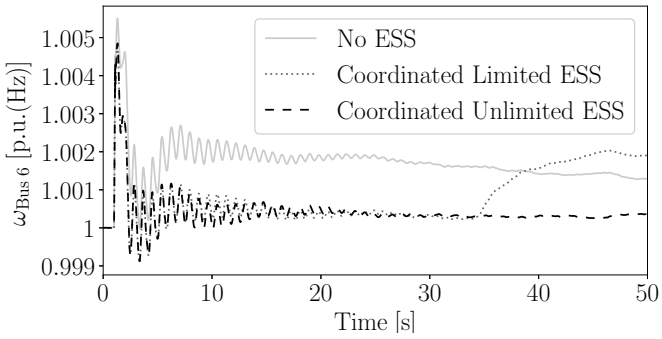

Fig. 10: Frequency response at bus 6 following the contingency with VPP after a mid-term.

control and with small (9 pu(MJ)) and large (30 pu(MJ)) energy capacity, respectively. Note that, in the case with small energy capacity, the ESS stops regulating the frequency at about $t = 35$ s and, as a consequence, the frequency deviation is even larger than in the case without ESS. This happens because, if the ESS is close to its maximum/minimum stored energy, the energy saturation/deficiency causes an abrupt transient oscillation [34]. This indicates that the size of the ESS is critical for the proper control of the VPP and its interaction with the rest of the system.

1) Stochastic Simulation: In this section, we consider stochastic variations of the wind speeds of 10% of the loads in the VPP. 500 Monte Carlo simulations are carried out for each of the four scenarios considered in this case study.

The capacity of the ESS included in the VPP is assumed to be small. The histogram and the best-fit probability density functions (PDF) are calculated at $t = 15$ s, as illustrated in Fig. 11, where σ is the standard deviation.

Comparing the standard deviation of $\omega_{\text{Bus 6}}$, σ, the VPP without frequency control on DERs shows a worse performance, where other three control schemes do not have significant differences. However, the coordinated ESS control scheme manages to recover the frequency closer to the reference value.

D. Impact of Communication Delays

The communication delays of the remote signal transmitted are taken into account in this section. Three levels of communication networks, namely high-speed, middle-speed, and low-speed communication network are considered. The settings of the communication networks are as follows. All the remote signal are considered as PMU data, transmitting through a Point-to-Point communication link. The packet size of PMU is 100 bytes, and the reporting rate is 25 frames per second. The communication protocol is UDP/IP to avoid the data retransmission and reduce the communication delay. Background traffic, e.g. the remote terminal unit (RTU) data and video surveillance streams, are also considered. The packet size and data rate of RTU data, video streams are 500 bytes, 1024 bytes, and 2 packets per second, 200 packets per second, respectively. Table I shows the parameters of the communication networks.

TABLE I: Parameters of the communication networks.

Levels	Bandwidth	PMU Data Rate	Background Traffic
High Speed	40 Mbps	25 frames/s	RTU, Video Stream
Middle Speed	4 Mbps	25 frames/s	RTU, Video Stream
Low Speed	0.4 Mbps	25 frames/s	N/A

The simulation results, in this case, are shown in Fig. 12. The responses with inclusion of communication delays are compared with the non-delay trajectory of Fig. 8. Fig. 12 also shows the impact of communication delays of the different communication network. The high-speed communication network has a better response compared to the other two.

The signal transmitted through a low-speed communication network has a more significant delay, which leads to a larger frequency deviation, even if the background traffic in such a network is ignored. Observe that the impact of communication networks in frequency response is nonlinear. The frequency deviation between the high-speed (40 Mbps) communication network and the middle-speed (4 Mbps) network is smaller than the deviation between the middle-speed network and the low-speed (0.4 Mbps) network, which means there exists a critical range of the bandwidth, over which increases the bandwidth can only slightly reduce communication delay. It is expected to find a suitable bandwidth of the communication network that the impact of delay on the system response is acceptable, and the cost of establishing a communication network is economical.

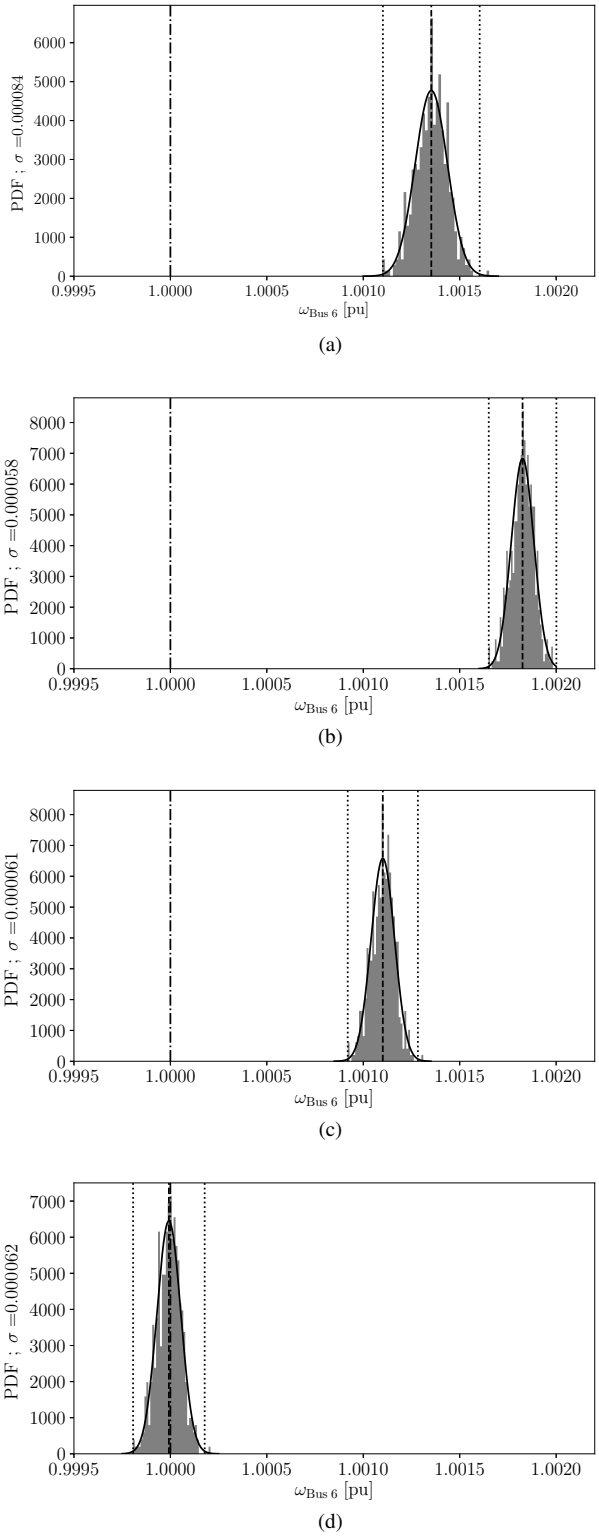

Fig. 11: Histogram and PDF-fit of the trajectories at $t = 15$ s: (a) no frequency control on DERs; (b) no ESS (c) non-coordinated ESS; (d) coordinated ESS.

VI. Conclusion

This paper studies the impact of VPPs on power system short-term dynamic response. Contingencies and stochastic

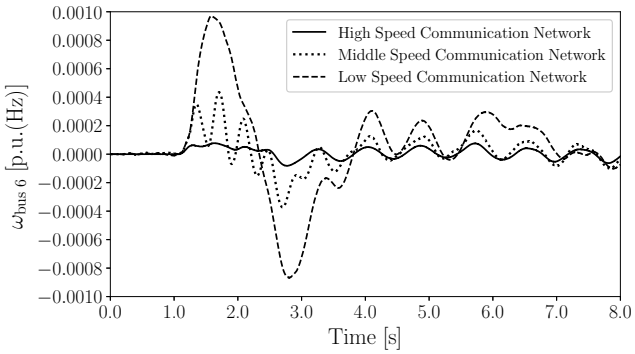

Fig. 12: Errors of the frequency at bus 6, the signal are transmitted in a different level communication network and compared with the non-delayed signal.

variations of the wind and voltage-dependent loads are considered. Simulation results indicate that the VPPs that coordinate the control of ESS and DERs shows a better frequency response compared to the case without coordinated control. Simulations also indicate that delays of different communication networks on the transient response have a small impact, which suggests that the coordinated control is feasible and its technology does not necessarily impact on the dynamic performance of the VPP.

Future work will focus on further developing the coordinated control scheme in VPP, e.g., secondary frequency control support by DGs through the coordinated active power output signal.

REFERENCES

[1] N. Ruiz, I. Cobelo, and J. Oyarzabal, "A direct load control model for virtual power plant management," *IEEE Trans. on Power Systems*, vol. 24, no. 2, pp. 959–966, 2009.

[2] E. Mashhour and S. M. Moghaddas-Tafreshi, "Bidding strategy of virtual power plant for participating in energy and spinning reserve markets – Part I: Problem formulation," *IEEE Trans. on Power Systems*, vol. 26, no. 2, pp. 949–956, 2011.

[3] M. Giuntoli and D. Poli, "Optimized thermal and electrical scheduling of a large scale virtual power plant in the presence of energy storages," *IEEE Trans. on Smart Grid*, vol. 4, no. 2, pp. 942–955, 2013.

[4] E. A. Setiawan, *Concept and Controllability of Virtual Power Plants*. Kassel University Press, 2007.

[5] H. Saboori, M. Mohammadi, and R. Taghe, "Virtual power plant (VPP), definition, concept, components and types," in *APEEC*, 2011, pp. 1–4.

[6] D. Pudjianto, C. Ramsay, and G. Strbac, "Virtual power plant and system integration of distributed energy resources," *IET Renewable Power Generation*, vol. 1, no. 1, pp. 10–16, 2007.

[7] H. Morais, M. Cardoso, L. Castanheira, and Z. Vale, "A decision-support simulation tool for virtual power producers," in *International Conference on Future Power Systems*, 2005, pp. 6–pp.

[8] F. Bignucolo, R. Caldon, V. Prandoni, S. Spelta, and M. Vezzola, "The voltage control on MV distribution networks with aggregated DG units (VPP)," in *International Universities Power Engineering Conference*, vol. 1, 2006, pp. 187–192.

[9] H. Morais, P. Kádár, M. Cardoso, Z. A. Vale, and H. Khodr, "VPP operating in the isolated grid," in *IEEE PES General Meeting*, 2008, pp. 1–6.

[10] H. Xin, D. Gan, N. Li, H. Li, and C. Dai, "Virtual power plant-based distributed control strategy for multiple distributed generators," *IET Control Theory & Applications*, vol. 7, no. 1, pp. 90–98, 2013.

[11] D. Koraki and K. Strunz, "Wind and solar power integration in electricity markets and distribution networks through service-centric virtual power plants," *IEEE Trans. on Power Systems*, vol. 33, no. 1, pp. 473–485, 2018.

[12] P. Moutis, P. S. Georgilakis, and N. D. Hatziargyriou, "Voltage regulation support along a distribution line by a virtual power plant based on a center of mass load modeling," *IEEE Trans. on Smart Grid*, vol. 9, no. 4, pp. 3029–3038, 2018.

[13] Y. Wang, X. Ai, Z. Tan, L. Yan, and S. Liu, "Interactive dispatch modes and bidding strategy of multiple virtual power plants based on demand response and game theory," *IEEE Trans. on Smart Grid*, vol. 7, no. 1, pp. 510–519, 2016.

[14] W. Liu, W. Gu, W. Sheng, X. Meng, Z. Wu, and W. Chen, "Decentralized multi-agent system-based cooperative frequency control for autonomous microgrids with communication constraints," *IEEE Trans. on Sustainable Energy*, vol. 5, no. 2, pp. 446–456, 2014.

[15] J.-Y. Kim, J.-H. Jeon, S.-K. Kim, C. Cho, J. H. Park, H.-M. Kim, and K.-Y. Nam, "Cooperative control strategy of energy storage system and microsources for stabilizing the microgrid during islanded operation," *IEEE Trans. on Power Electronics*, vol. 25, no. 12, pp. 3037–3048, 2010.

[16] N. Etherden, V. Vyatkin, and M. H. Bollen, "Virtual power plant for grid services using IEC 61850," *IEEE Trans. on Industrial Informatics*, vol. 12, no. 1, pp. 437–447, 2015.

[17] H. Yang, D. Yi, J. Zhao, and Z. Dong, "Distributed optimal dispatch of virtual power plant via limited communication," *IEEE Trans. on Power Systems*, vol. 28, no. 3, pp. 3511–3512, 2013.

[18] X. Sui, Y. Tang, H. He, and J. Wen, "Energy-storage-based low-frequency oscillation damping control using particle swarm optimization and heuristic dynamic programming," *IEEE Trans. on Power Systems*, vol. 29, no. 5, pp. 2539–2548, 2014.

[19] B. C. Pal, A. H. Coonick, I. M. Jaimoukha, and H. El-Zobaidi, "A linear matrix inequality approach to robust damping control design in power systems with superconducting magnetic energy storage device," *IEEE Trans. on power systems*, vol. 15, no. 1, pp. 356–362, 2000.

[20] J. Morren, S. W. De Haan, W. L. Kling, and J. Ferreira, "Wind turbines emulating inertia and supporting primary frequency control," *IEEE Trans. on power systems*, vol. 21, no. 1, pp. 433–434, 2006.

[21] Á. Ortega and F. Milano, "Impact of frequency estimation for VSC-based devices with primary frequency control," in *ISGT-Europe*, 2017, pp. 1–6.

[22] B. Tamimi, C. Cañizares, and K. Bhattacharya, "Modeling and performance analysis of large solar photo-voltaic generation on voltage stability and inter-area oscillations," in *IEEE PES General Meeting*, 2011, pp. 1–6.

[23] A. Nicastri and A. Nagliero, "Comparison and evaluation of the PLL techniques for the design of the grid-connected inverter systems," in *ISIE*, 2010, pp. 3865–3870.

[24] F. Milano and M. Anghel, "Impact of time delays on power system stability," *IEEE Trans. on Circuits and Systems I: Regular Papers*, vol. 59, no. 4, pp. 889–900, 2011.

[25] B. Naduvathuparambil, M. C. Valenti, and A. Feliachi, "Communication delays in wide area measurement systems," in *Southeastern Symposium on System Theory*, 2002, pp. 118–122.

[26] M. Liu and F. Milano, "Small-signal stability analysis of power systems with inclusion of periodic time-varying delays," in *PSCC*, 2018, pp. 1–7.

[27] M. Liu, I. Dassios, G. Tzounas, and F. Milano, "Stability analysis of power systems with inclusion of realistic-modeling wams delays," *IEEE Trans. on Power Systems*, vol. 34, no. 1, pp. 627–636, 2018.

[28] W. Zhong, M. Liu, and F. Milano, "A co-simulation framework for power systems and communication networks," in *PowerTech*, 2019, pp. 1–6.

[29] F. Milano and R. Zárate-Miñano, "A systematic method to model power systems as stochastic differential algebraic equations," *IEEE Trans. on Power Systems*, vol. 28, no. 4, pp. 4537–4544, 2013.

[30] R. Zárate-Minano, F. M. Mele, and F. Milano, "SDE-based wind speed models with weibull distribution and exponential autocorrelation," in *IEEE PES General Meeting*, 2016, pp. 1–5.

[31] P. W. Sauer and M. A. Pai, *Power System Dynamics and Stability*. Prentice Hall, 1998, vol. 101.

[32] C. Murphy and A. Keane, "Local and remote estimations using fitted polynomials in distribution systems," *IEEE Trans. on Power Systems*, vol. 32, no. 4, pp. 3185–3194, 2016.

[33] F. Milano, "A Python-based software tool for power system analysis," in *IEEE PES General Meeting*, 2013, pp. 1–5.

[34] A. Ortega and F. Milano, "Design of a control limiter to improve the dynamic response of energy storage systems," in *IEEE PES General Meeting*, 2015, pp. 1–5.